Graphene for Hydrogen Generation

DOI: 10.1002/ange.201304505

P-Doped Graphene Obtained by Pyrolysis of Modified Alginate as a Photocatalyst for Hydrogen Generation from Water–Methanol Mixtures**

Marcos Latorre-Sánchez, Ana Primo, and Hermenegildo García**

Graphene and related materials offer many possibilities for applications in microelectronics[1–4] and as advanced carbocatalysts.[5–8] It has also been reported that, depending on the degree of oxidation, graphene oxide (GO) can act as a photocatalyst for H_2 generation under UV illumination.[4,9–14] Dye sensitization leads to a visible-light response in GO for H_2 generation.[15] Compared to conventional TiO_2 and inorganic semiconductors, the use of graphene-like materials as photocatalysts is advantageous because of their wide availability, sustainability when graphene is prepared from renewable resources, and easy derivatization, which can eventually increase their photocatalytic activity.[3,13,14] Continuing with the exploitation of the potential of graphene-based materials as photocatalysts, we herein report the photocatalytic activity for phosphorus-doped graphene ((P)G) in H_2 generation. This material can be conveniently and reproducibly prepared from biomass, and exhibits an activity about nine times higher than that of GO. Moreover, (P)G exhibits visible-light photocatalytic activity. These results may lead to the development of a new generation of graphene-based photocatalysts by using doped materials.

Preparation of (P)G was accomplished by pyrolysis of $H_2PO_4^-$-modified alginate at 900 °C under inert atmosphere. Alginate is a natural oligosaccharide that consists of unbranched chains of condensed guluronic and mannuronic acid units that are linked through 1,4-glycoside bonds (Scheme 1). Various amounts of $H_2PO_4^-$ (20–320 wt. % with respect to alginate) were added to aqueous solutions of alginate at neutral pH. Alginate particles suspended in water adsorbed some $H_2PO_4^-$, as the zeta potential of the alginate solutions varied from −75 mV to −59 mV, depending on the percentage of $H_2PO_4^-$ added. The resulting alginate hydrogel that embedded $H_2PO_4^-$ was collected from water and pyrolyzed under an Ar atmosphere (Scheme 1). During the pyrolysis, the phosphate-containing alginate, which was originally white, became a black solid, which indicates

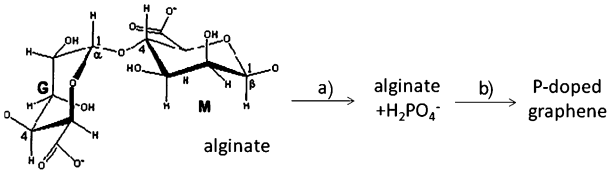

Scheme 1. Preparation of (P)G. a) Addition of $H_2PO_4^-$ to a colloidal solution of alginate at neutral pH, and recovery of the solid. b) Pyrolysis of phosphate-containing alginate at 900 °C under an Ar atmosphere, and extended sonication. A simplified structure of natural alginate, which is composed of mannuronic (M) and guluronic (G) monosaccharides, is shown.

graphitization of the polysaccharide. At the same time, a yellow-red solid was formed and deposited on the furnace walls. This sublimed material was characterized by XRD as elemental phosphorus, which was generated by in situ thermal reduction of the phosphate by the graphitic carbon residue formed from alginate. The amount of sublimed phosphorus increased with the amount of phosphate added to alginate. (P)G can finally be obtained by sonication of the graphitic residue in water (for an SEM image of this graphitic residue, see the Supporting Information, Figure S1). We have previously observed that graphitic residues from some natural polymers can be easily exfoliated by sonication without oxidation, as required for crystalline graphite.[16] The yield of (P)G from the pyrolysis of modified alginate was estimated as 62 % from the residual weight after four consecutive sonication cycles.

Four (P)G samples with a different $H_2PO_4^-$content were prepared (Table 1). The amount of P doping increased only slightly even when the $H_2PO_4^-$ dosage was increased from 0.1 to 1.6 g (Table 1). After pyrolysis, the carbonaceous residues were characterized by UV/Vis, Raman, and ^{31}P NMR spec-

[*] M. Latorre-Sánchez, Dr. A. Primo, Prof. H. García
Instituto Universitario de Tecnología Química
Univ. Politécnica de Valencia
Av. De los Naranjos s/n, 46022 Valencia (Spain)
E-mail: aprimoar@itq.upv.es
hgarcia@qim.upv.es

[**] Financial Support by the Spanish Ministry of Economy and Competitiveness (Severo Ochoa and CTQ2012-32315) is gratefully acknowledged. M.L. and A.P. also thank the Spanish Ministry and the National Research Council for a postgraduate scholarship and a research-associate contract, respectively.

Supporting information for this article is available on the WWW under http://dx.doi.org/10.1002/anie.201304505.

Table 1: Graphene samples used in the present study, and selected analytical data obtained by XPS.

Sample	HPO_4^{2-} [g][a]	Atomic ratio[b]	
		C [%]/O [%]	C [%]/P [%]
Graphene	–	3.09	–
(P)G-1[c]	0.1	4.67	17.16
(P)G-2	0.2	6.95	13.86
(P)G-3	0.8	11.5	13.95
(P)G-4[d]	1.6	32.19	12.73

[a] The amount of HPO_4^{2-} added in step (a). [b] Atomic ratios of graphenic C [%] with O or P doping [%]. [c] Brunauer–Emmett–Teller (BET) surface area = 109 $m^2 g^{-1}$. [d] BET surface area = 80 $m^2 g^{-1}$.

troscopy, X-ray photoelectron spectroscopy (XPS), and electron microscopy. UV/Vis optical spectroscopy showed a typical absorption spectrum with an extinction coefficient that increases towards the blue side of the visible region, and a band at $\lambda_{max} = 265$ nm in the UV region (Figure 1; see also the Supporting Information, Figure S2). Raman spectroscopy

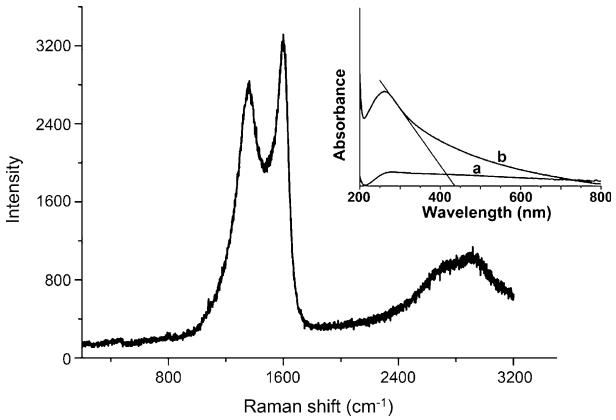

Figure 1. Raman spectrum of (P)G-2 recorded using a wavelength of 514 nm for excitation. Inset: Comparison of the UV/Vis spectra of graphene (a) and (P)G-2 (b; see Table 1). The optical band gap for (P)G-2 was estimated from the onset of the 265 nm band.

is a suitable characterization technique for graphitic materials.[17–19] The Raman spectrum recorded for a (P)G-2 sample showed the three expected peaks that correspond to the 2D′ band (2892 cm^{-1}), and the G and D peaks (1596 and 1358 cm^{-1}, respectively; Figure 1). The presence of P atoms, and the fact that they are incorporated into the graphene sheet was ascertained by XPS measurements and solid-state ^{31}P NMR spectroscopy. As an example, Figure 2 shows the C1s and P2p peaks recorded for (P)G-2. Deconvolution of

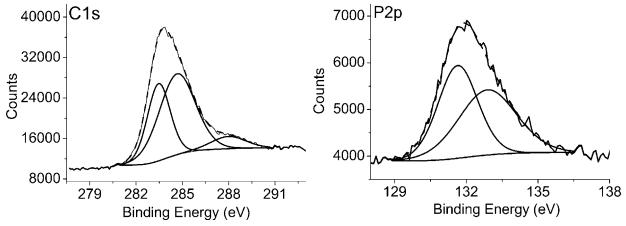

Figure 2. C1s and P2p peaks recorded for (P)G-2 by XPS, and their corresponding best deconvolution fits.

the C1s peak leads to three components at binding energies of 288.1, 284.7, and 283.5 eV that correspond to C atoms bonded to O atoms, graphenic C atoms, and graphenic C atoms connected to P atoms, respectively. The percentage of the component corresponding to C atoms bonded to O atoms decreases significantly with the percentage of the phosphate in the modified alginate precursor and with a concomitant increase in the percentage of graphenic C atoms. This trend that was observed by XPS of the series indicates that the quality of the graphene sheet increases without a large increase in the P-doping level when the alginate precursor contains a larger proportion of phosphate. We correlate this increase in the quality of the graphene sheets to the observation that elemental phosphorus was evolved in the furnace. We propose that these C atoms bonded to O atoms are those that preferably evolve as CO_2 during the reduction of phosphate by elemental carbon to elemental phosphorus. The increase in the percentage of graphene C atoms has an influence on the photocatalytic activity of the material for H_2 generation from water/methanol mixtures as presented below. The P2p peak was deconvoluted into two components of binding energies of 132.9 and 131.5 eV that are clearly different to the binding energy of phosphate, which appears at 134.1 eV, and can be attributed to P atoms bonded to O atoms and C atoms, respectively. A third peak that indicates the presence of oxygen was also recorded. In a recent report on P-doped graphite layers that were obtained by the oven pyrolysis of triphenylphosphine in toluene at 1000 °C, XPS peaks at binding energies almost coincident to those observed here for (P)G were observed.[20] In agreement with the deconvolution of the P2p peak observed by XPS, the ^{31}P NMR spectrum of (P)G-2 (Supporting Information, Figure S3) entailed two peaks at −4 and 21 ppm; these are attributable to the two types of P and match well with the expected values for PPh_3 and $O{=}PPh_3$ that appear at −6 and 23 ppm, respectively, in solution.

The typical graphene morphology with the expected hexagonal arrangement of C atoms, and the absence of carbon particles from pyrolized alginate residues, was observed by electron microscopy of the (P)G material suspended in water. Selected TEM images recorded after drop-casting a suspended (P)G-2 sample are shown in Figure 3. Selected-area electron diffraction (SAED) of this sample shows a pattern that corresponds to the hexagonal

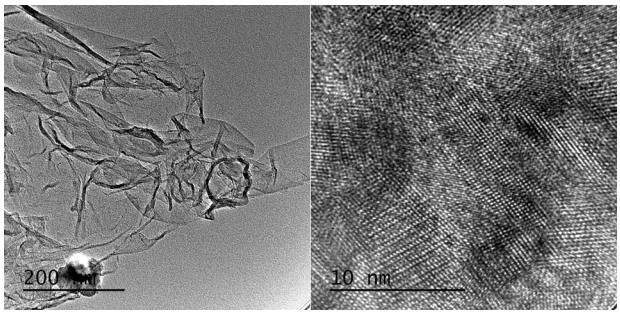

Figure 3. TEM (left) and high-resolution TEM (right) images of (P)G-2. The scale bars correspond to 200 nm and 10 nm for the left and right panels, respectively.

monocrystalline domains in the material. Overall, the characterization data is in agreement with the formation of graphene and simultaneous P doping upon pyrolysis of the natural polysaccharide alginate, and sonication in water. P doping of graphene starting from the phosphate can be envisioned as a two-step process that requires the reduction of PO_4^{3-} to elemental phosphorus, and a subsequent reaction of the elemental phosphorus with graphene. Generation of

elemental phosphorus in the pyrolysis was particularly notable for the samples with the highest phosphate content. The substitution of C atoms by P atoms in the graphene sheets was confirmed by the binding energies for the P2p peak in XPS that coincide with those reported for P-doped graphene,[20] by ^{31}P NMR spectroscopy, in which peaks that correspond to P atoms bonded to C atoms at −4 and 21 ppm were recorded, and by the C1s component that was found to occur at lower binding energies than C atoms of graphene attributable to C atoms bonded to P atoms by XPS.[21]

The monolayer morphology of (P)G suspended in water was assessed by measuring the vertical height of the platelets (average dimensions of $1 \times 2\ \mu m^2$), which was found to vary from 0.5 to 2.2 nm by AFM, depending on the wrinkles of the sheet (Supporting Information, Figure S4).

As explained in the introduction, the purpose of this work was to determine the activity of (P)G for H_2 generation upon irradiation in water and in the presence of sacrificial electron donors. Photocatalytic irradiations were carried out using UV/Vis light from a Xe lamp. In water/methanol mixtures, the amount of H_2 evolved increases significantly with the percentage of $H_2PO_4^-$ introduced during the synthesis of (P)G; the maximum photocatalytic activity was obtained for the sample prepared with the maximum percentage of $H_2PO_4^-$. The results obtained are shown in Figure 4. For the sake of comparison, a sample of GO that was prepared by the oxidation of graphite and subsequent exfoliation, as well as a graphene sample obtained by the pyrolysis of alginate at 900 °C, and reconstituted graphene (rG) that was obtained by the reduction of GO were included in our study. The graphene material prepared as (P)G but in the absence of $H_2PO_4^-$ exhibited the lowest photocatalytic activity for H_2 evolution, which is in agreement with its conducting nature (Figure 4a). GO exhibits a photocatalytic activity approximately three times higher than graphene. Notably, the presence of P atoms increases the photocatalytic activity by more than one order of magnitude, and the activity of GO was thus significantly lower than that of (P)G.

To determine if the photocatalytic activity of P(G) derives exclusively from the UV region, or if (P)G also exhibits visible-light photoresponse, we employed a similar photocatalytic test, but used filtered light of wavelengths longer than 390 nm. The H_2-generation activity of the series of photocatalysts under visible-light irradiation in water/methanol mixtures is also shown in Figure 4. Only (P)G-2, (P)G-3, and (P)G-4 display a residual visible-light photocatalytic activity, while the rest of the samples are photocatalytically inactive under these conditions. However, a comparison of the H_2 generation activity under UV/Vis and visible-light irradiation leads to the conclusion that a large percentage of H_2 evolved under UV/Vis irradiation must derive from UV-light excitation, and that there is still room for improving the activity under visible-light irradiation. According to the UV/Vis spectra, the optical bandgap, which was estimated from the onset of the absorption band, grows from 0 eV for graphene to 2.85 eV for (P)G-4 (Figure 1, inset; Supporting Information, Figure S2).

The previous data on the photocatalytic activity were measured in water/methanol mixtures for (P)G samples that

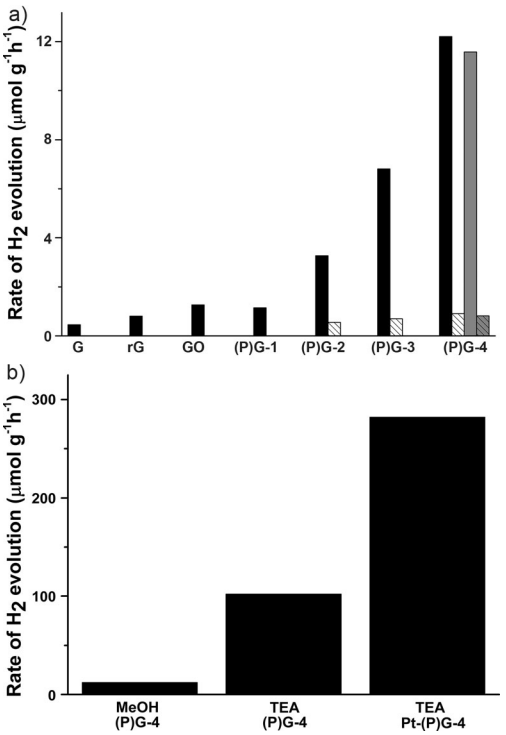

Figure 4. a) Photocatalytic activity for H_2 generation for samples of graphene, rG, GO, (P)G-1, (P)G-2, (P)G-3, (P)G-4, and (P)G-4 (third use) from an aqueous methanol solution (30 v/v%). Catalyst concentration = 0.16 g L^{-1}. Black: irradiation with UV/Vis light; shaded white: irradiation with visible light (> 390 nm); gray: irradiation with UV/Vis light, third use of the catalyst; shaded gray: irradiation with visible light (> 390 nm), third use of the catalyst. Graphene, rG, GO, and (P)G-1 do not exhibit measurable photocatalytic activity under visible-light irradiation. b) The H_2 production rate for (P)G-4 in MeOH and triethanolamine (TEA), and for Pt–(P)G-4 in TEA under UV/Vis irradiation.

lacked Pt as H_2 evolution center. For a facilitated comparison with previously reported data,[22] we also measured the photocatalytic activity using triethanolamine, which is a better sacrificial electron donor than methanol. We also tested the photocatalytic activity for a sample containing Pt nanoparticles (Pt–(P)G-4). Pt–(P)G-4 (Pt nanoparticles of an average size of 2 nm; for TEM images, see the Supporting Information, Figure S5) was prepared by photochemical deposition by irradiating a water/methanol suspension of (P)G-4 in the presence of $H_2[PtCl_6]$ (see the Supporting Information). Irradiation using Pt–(P)G in triethanolamine increases the photocatalytic activity of (P)G-4 by a factor of 23.5 and 14.1 for UV/Vis and filtered-light irradiation, respectively (Supporting Information, Section S6; Figure 4b). The highest H_2-generation rate was 282 $\mu mol\, g^{-1} h^{-1}$ for Pt–(P)G-4 under UV/Vis irradiation using triethanolamine. These values for the production rate of H_2 are comparable to those previously reported in the literature for carbon–nitride photocatalysts,[22] and clearly show that doping is a valid strategy to introduce photocatalytic activity into graphene materials.

One concern when using graphene-like materials as a photocatalyst is their stability under the irradiation con-

ditions. To address this issue, we recovered the catalyst after 23 h of irradiation, washed and reused for a second and third run under the same experimental conditions under UV/Vis and visible-light illumination in water/methanol mixtures. Recycling the catalyst three times led to a decrease of 5% and 10% depending on whether the irradiation was carried out with UV/Vis or visible light, respectively (Figure 4). This decrease can probably be attributed to the incomplete recovery of the (P)G photocatalyst, although some degree of deactivation might be due to the stacking of layers or the decomposition of some active sites, considering the visual observation of the formation of some precipitate. XPS measurements of the photocatalyst that was reused three times do not show significant differences for the C and P peaks compared with the original fresh (P)G sample, which suggests that decomposition of the material is not the cause of this minor decrease in the activity.

It has been proposed that the photocatalytic activity of GO arises from its semiconducting nature, as zero-bandgap graphene does not exhibit photocatalytic activity.[4] In the present case, the presence of P atoms should make the resulting (P)G semiconducting, and accordingly, the activity of (P)G would arise from the presence of P atoms in combination with a high-quality graphene structure as observed by XPS of the C1s peak. Theoretical calculations with N and B doping in ideal graphene sheets have shown that doping must convert graphene from a conductor to a semiconductor with a tunable bandgap that should increase with the doping percentage.[23] In the present case, the optical bandgap and the photocatalytic activity of P(G) grow with the P content, which is in line with these calculations.

In conclusion, we have disclosed a simple method for the preparation of P-doped graphene by the pyrolysis of abundant and natural alginate conjugated with $H_2PO_4^-$ in the absence of oxygen. P doping has been inferred from XPS and ^{31}P NMR measurements. We have determined that an increase in the amount of HPO_4^{2-} increases the photocatalytic activity for H_2 generation from water/methanol mixtures with respect to analogous graphene materials that do not contain P atoms, by reducing the defect density. Furthermore, the photocatalytic activity of (P)G is about one order of magnitude higher than that of GO, the activity of which is significantly enhanced by using good sacrificial electron donors (triethanolamine), and by the presence of Pt. Importantly, (P)G also exhibits H_2-evolution activity that is absent for the other three control materials under visible-light irradiation.

Overall, the ease with which doped graphene materials can be obtained from natural polysasacharides by conjugation of a suitable dopant precursor has been shown. It is very likely that this method can also become suitable for the preparation of many other doped graphene materials.[24] These structures could exhibit improved performance induced by the presence of heteroatoms, as herein described for a photocatalytic application.

Received: May 24, 2013
Revised: July 4, 2013
Published online: September 17, 2013

Keywords: graphene · hydrogen · phosphorus · photocatalysis · solar fuels

[1] A. K. Geim, *Science* **2009**, *324*, 1530 – 1534.
[2] A. K. Geim, K. S. Novoselov, *Nat. Mater.* **2007**, *6*, 183 – 191.
[3] Q. J. Xiang, J. G. Yu, M. Jaroniec, *Chem. Soc. Rev.* **2012**, *41*, 782 – 796.
[4] T.-F. Yeh, J.-M. Syu, C. Cheng, T.-H. Chang, H. Teng, *Adv. Funct. Mater.* **2010**, *20*, 2255 – 2262.
[5] D. R. Dreyer, H. P. Jia, A. D. Todd, J. Geng, C. W. Bielawski, *Org. Biomol. Chem.* **2011**, *9*, 7292 – 7295.
[6] D. R. Dreyer, C. W. Bielawski, *Chem. Sci.* **2011**, *2*, 1233 – 1240.
[7] H. P. Jia, D. R. Dreyer, C. W. Bielawski, *Tetrahedron* **2011**, *67*, 4431 – 4434.
[8] D. R. Dreyer, H. P. Jia, C. W. Bielawski, *Angew. Chem.* **2010**, *122*, 6965 – 6968; *Angew. Chem. Int. Ed.* **2010**, *49*, 6813 – 6816.
[9] X. Q. An, J. C. Yu, *RSC Adv.* **2011**, *1*, 1426 – 1434.
[10] C. C. Huang, C. Li, G. Q. Shi, *Energy Environ. Sci.* **2012**, *5*, 8848 – 8868.
[11] Y. T. Liang, M. C. Hersam, *Macromol. Chem. Phys.* **2012**, *213*, 1091 – 1100.
[12] B. F. Machado, P. Serp, *Catal. Sci. Technol.* **2012**, *2*, 54 – 75.
[13] J. J. Vilatela, D. Eder, *ChemSusChem* **2012**, *5*, 456 – 478.
[14] N. Zhang, Y. H. Zhang, Y. J. Xu, *Nanoscale* **2012**, *4*, 5792 – 5813.
[15] M. Latorre-Sánchez, C. Lavorato, M. Puche, V. Fornés, R. Molinari, H. Garcia, *Chem. Eur. J.* **2012**, *18*, 16774 – 16783.
[16] A. Primo, A. Forneli, A. Corma, H. Garcia, *ChemSusChem* **2012**, *5*, 2207 – 2214.
[17] A. C. Ferrari, *Solid State Commun.* **2007**, *143*, 47 – 57.
[18] L. M. Malard, M. A. Pimenta, G. Dresselhaus, M. S. Dresselhaus, *Phys. Rep.* **2009**, *473*, 51 – 87.
[19] R. Saito, M. Hofmann, G. Dresselhaus, A. Jorio, M. S. Dresselhaus, *Adv. Phys.* **2011**, *60*, 413 – 550.
[20] Z. W. Liu, F. Peng, H. J. Wang, H. Yu, W. X. Zheng, J. Yang, *Angew. Chem.* **2011**, *123*, 3315 – 3319; *Angew. Chem. Int. Ed.* **2011**, *50*, 3257 – 3261.
[21] J. C. Han, A. P. Liu, J. Q. Zhu, M. L. Tan, H. P. Wu, *Appl. Phys. A* **2007**, *88*, 341 – 345.
[22] X. Wang, K. Maeda, A. Thomas, K. Takanabe, G. Xin, J. M. Carlsson, K. Domen, M. Antonietti, *Nat. Mater.* **2009**, *8*, 76 – 80.
[23] P. Rani, V. K. Jindal, *RSC Adv.* **2013**, *3*, 802 – 812.
[24] Preliminary data show that B^- and S^- doping can also be performed in a similar fashion; these results will be reported in due course.